analytical chemistry

pubs.acs.org/ac Article

A Fluorescent Probe with Zwitterionic ESIPT Feature for Ratiometric Monitoring of Peroxynitrite In Vitro and In Vivo

Zhenkai Wang,[‖] Miao Yan,[‖] Miaomiao Yu, Gang Zhang, Weiwei Fang,* and Fabiao Yu*

Cite This: *Anal. Chem.* 2024, 96, 3600−3608 Read Online

ACCESS | Metrics & More | Article Recommendations | Supporting Information

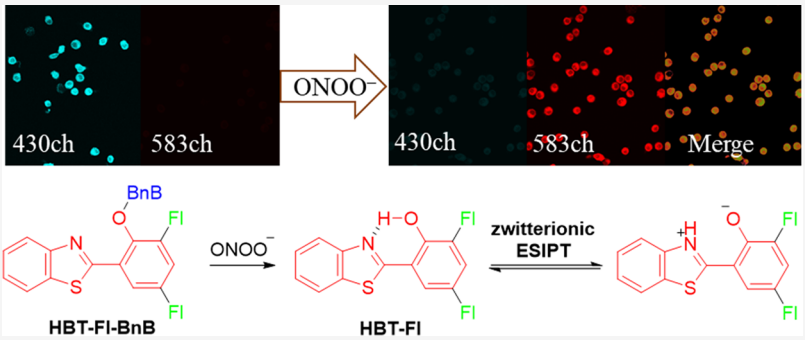

ABSTRACT: Peroxynitrite ($ONOO^-$), as a short-term reactive biological oxidant, could lead to a series of effects in various physiological and pathological processes due to its subtle concentration changes. In vivo monitoring of $ONOO^-$ and relevant physiological processes is urgently required. Herein, we describe a novel fluorescent probe termed **HBT-Fl-BnB** for the ratiometric detection of $ONOO^-$ in vitro and in vivo. The probe consists of an HBT core with Fl groups at the ortho and para positions responding to the zwitterionic excited-state intramolecular proton-transfer (zwitterionic ESIPT) process and a boronic acid pinacol ester with dual roles that block the zwitterionic ESIPT and recognize $ONOO^-$. Thanks to the specificity as well as low cytotoxicity, success in imaging of endogenous and exogenous $ONOO^-$ in living cells by **HBT-Fl-BnB** was obtained. Additionally, the applicability of **HBT-Fl-BnB** to tracking the abnormal expression of $ONOO^-$ in vivo induced by inactivated *Escherichia coli* was also explored. This is the first report of a fluorescent probe for $ONOO^-$ sensing via a zwitterionic ESIPT mechanism.

INTRODUCTION

Endogenous peroxynitrite ($ONOO^-$) has been recognized as a strong oxidant in physiological processes, rendering itself as a central biological pathogenic factor in a plethora of pathophysiological changes, such as cardiovascular, neurodegenerative, and inflammatory disorders.[1−3] Besides, as a member of the reactive nitrogen species (RNS), $ONOO^-$ is also deemed to be a nitrating agent, which not only causes nitrative stress in vivo but also acts as the biomarker via the nitration of biomacromolecules, thereby altering the cellular processes.[4−6] It is typically observed in numerous clinical diseases, such as Alzheimer's disease, Parkinson's disease, cancer, and autoimmune disease of the central nervous system.[7−9] Considering its unique characteristic such as subtle change of concentration level (nM to mM), ultrashort half-lifetime (∼20 ms), and high reactivity (oxidative and nucleophilic abilities), it is still a challenge to realize the comprehensive detection of $ONOO^-$. Therefore, to gain a deep insight of its paradoxical role in biological systems, it is of great importance to develop an effective approach for accurate detection of $ONOO^-$, which remains a challenging task.[10,11]

Until now, small molecular fluorescent probes are emerging as the most powerful tool for imaging $ONOO^-$ in vitro/in vivo due to their unique characteristics of high sensitivity, specificity, noninvasiveness, and great temporal and spatial resolutions.[12−19] Among them, excited-state intramolecular proton-transfer (ESIPT)-based probes reveal a promising applicability featuring with good photostability, large Stokes shift, and ratiometric capability.[20−22] Among them, functionalized 2-phenylbenzothiazole including 2-(2′-aminophenyl)-benzothiazole (ABT)[23−25] and 2-(2′-hydroxyphenyl)-benzothiazole (HBT),[26−36] as the classical ESIPT chromophores, were well developed, which would advance the phototautomerization switching between the enol and keto forms (named as π-delocalized ESIPT) after the release of the sensing moiety for $ONOO^-$. For instance, Hu and co-workers developed a fluorescent switch-on probe by incorporating the *p*-hydroxyaniline moiety into the ABT skeleton, and the

Received: December 15, 2023
Revised: January 24, 2024
Accepted: January 31, 2024
Published: February 19, 2024

https://doi.org/10.1021/acs.analchem.3c05718
Anal. Chem. 2024, 96, 3600−3608

oxidative cleavage of *p*-hydroxyaniline exerted by $ONOO^-$ released the fluorescent ABT core, realizing the monitoring of $ONOO^-$ in vitro and in vivo.[23] The simultaneous introduction of phenothiazine-based coumarin and benzyl boronic ester moieties (BnB) into ABT rendered the probe to detect ClO^- and $ONOO^-$ through two distinct emission channels with fast responses.[25] James and other groups presented a series of HBT-derived fluorescent probes realizing the ratiometric sensing of $ONOO^-$ in vitro and in vivo.[26−36] Despite these achievements, only few reports with emission wavelengths for the keto forms of π-delocalized ESIPT chromophores were longer than 550 nm.[30,32] In sharp contrast, fluorescent probes featuring the zwitterionic ESIPT mechanism are not reported currently, though it might endow probe molecules with emission at long wavelengths.[37]

In this sense, the zwitterionic ESIPT mechanism is quite different from the conventional π-delocalized one. In a word, zwitterionic ESIPT process would undergo a charge redistribution to acquire a zwitterionic form, which consisted of a positively charged and a negatively charged moiety, favoring the proton transfer. According to previous studies, it would endow the fluorescent materials with remarkably larger Stokes shifts with a pronounced redshift in the emission spectra in comparison with theb classical π-delocalized ESIPT.[38,39] Given its unique spectra property, herein, we present a rationally designed ratiometric fluorescent probe featuring zwitterionic ESIPT mechanism for $ONOO^-$ based on the HBT core, termed as **HBT-FI-BnB**. As shown in Scheme 1, the structure

Scheme 1. Designed HBT-Fl-BnB and Its Relevant Synthetic Route

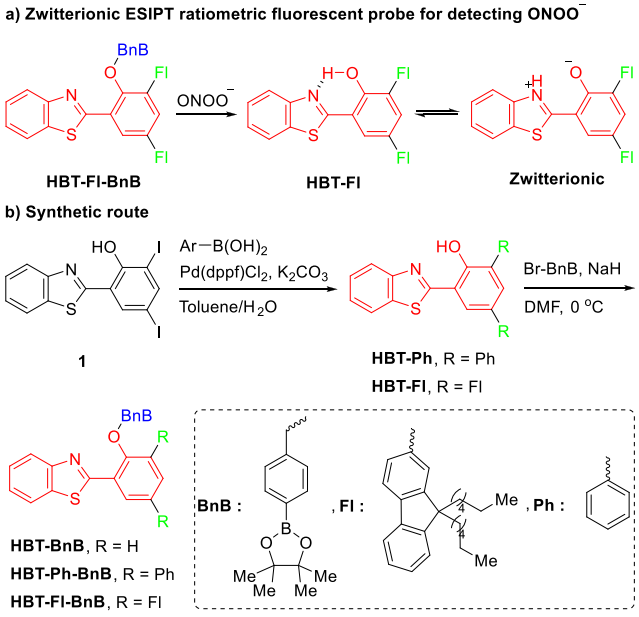

of **HBT-FI-BnB** consisted of BnB and two fluorenyl (Fl) units at the ortho and para positions (relative to OH) of the HBT chromophore. Consequently, this probe exhibited an emission with λ_{max} at 396 nm, and this peak remarkably decreased with a concomitant new emission at 583 nm in the presence of $ONOO^-$. Then, it was successfully applied to the fluorescent imaging of exogenous and endogenous $ONOO^-$ in living Raw264.7 cells. Importantly, the inactivated *Escherichia coli*-induced expression of $ONOO^-$ in mice was also feasibly monitored by **HBT-FI-BnB**, presenting a potential tool for elucidating its relevant pathogenic mechanism. To the best of our knowledge, this is the first report on a fluorescent probe with a zwitterionic ESIPT mechanism, providing a novel platform for ratiometric sensing of $ONOO^-$.

EXPERIMENTAL SECTION

Design and Synthesis of Probe HBT-R-BnB. *Synthesis of Probe HBT-BnB.* To a Schlenk tube containing HBT (227 mg, 1 mmol) in dry DMF (15 mL) was added NaH (60% in mineral oil, 44 mg, 1.1 mmol) in portions at 0 °C, and the mixture was stirred for 0.5 h. Then, a solution of 4-bromomethylphenylboronic acid pinacol ester (327 mg, 1.1 mmol) in dry DMF (3 mL) was added dropwise at 0 °C. The reaction mixture was stirred at room temperature for 8 h. Then, it was poured into ice water, leading to the precipitation of crude products. **HBT-BnB** as a white solid (204 mg, 46% yield) was obtained via purification by using silica gel column chromatography (petroleum ether/dichloromethane as eluents, v/v = 2:1).

^{1}H NMR (600 MHz, $CDCl_3$, ppm): δ = 8.55 (d, J = 7.8 Hz, 1H), 8.09 (d, J = 8.1 Hz, 1H), 7.89 (d, J = 7.9 Hz, 1H), 7.86 (d, J = 7.6 Hz, 2H), 7.48 (t, J = 7.1 Hz, 1H), 7.40 (t, J = 2.9 Hz, 1H), 7.36 (t, J = 4.0 Hz, 1H), 7.13 (t, J = 7.2 Hz, 1H), 7.08 (d, J = 8.3 Hz, 1H), 5.36 (s, 2H), 1.36 (s, 12H). ^{13}C NMR (150 MHz, $CDCl_3$, ppm): δ = 163.1, 156.3, 152.2, 139.2, 135.1, 131.7, 129.8, 127.0, 125.9, 124.6, 122.8, 121.5, 121.4, 113.0, 83.9, 71.0. HR-MS (ESI, m/z): calcd for $C_{27}H_{27}NO_3S$ $[M + H]^+$: 444.1805, found: 444.1800.

Synthesis of probe HBT-Ph-BnB. To a 100 mL Schlenk flask with a magnetic stirrer were added 2-(benzo[d]thiazol-2-yl)-4,6-diiodophenol (479 mg, 1 mmol), phenyl boronic acid (366 mg, 3 mmol), potassium carbonate (1.1 g, 8 mmol), and 1,1′-bis(diphenylphosphino)ferrocene-palladium(II)-dichloride dichloromethane complex (30 mg, 0.037 mmol) under N_2, followed by the addition of toluene/H_2O mixture (5 mL/2.5 mL). The reaction mixture was bubbled with N_2 for 10 min and was heated to reflux at 120 °C for 17 h. After being cooled to room temperature, water and petroleum ether were added, and the organic layer was separated. It was filtered by passing through a pad of Celite and washed with additional petroleum ether. The filtrate was evaporated under reduced pressure and was further purified by using silica gel column chromatography (petroleum/dichloromethane as eluents, v/v = 10:1), affording desired **HBT-Ph** as a white solid (364 mg, 96%).

^{1}H NMR (600 MHz, $CDCl_3$, ppm): δ = 13.19 (s, 1H), 7.96 (d, J = 8.1 Hz, 1H), 7.93 (d, J = 7.9 Hz, 1H), 7.91 (d, J = 1.2 Hz, 1H), 7.72 (t, J = 6.0 Hz, 3H), 7.65 (d, J = 2.7 Hz, 2H), 7.53−7.48 (m, 5H), 7.45−7.37 (m, 3H). ^{13}C NMR (150 MHz, $CDCl_3$, ppm): δ = 169.7, 154.9, 151.8, 140.2, 169.7, 154.97, 151.8, 140.2, 137.9, 132.9, 132.82, 132.79, 131.3, 129.6, 129.1, 128.3, 127.6, 127.3, 126.9, 126.1, 125.8, 122.3, 121.7, 117.3. HR-MS (ESI, m/z): calcd for $C_{26}H_{19}NOS$ $[M + H]^+$: 380.1109, found: 380.1087.

To a Schlenk tube containing **HBT-Ph** (87 mg, 0.23 mmol) in dry DMF (15 mL) was added NaH (60% in mineral oil, 10 mg, 0.25 mmol) in portions at 0 °C. Then, the mixture was stirred for 0.5 h. A solution of 4-bromomethylphenylboronic acid pinacol ester (75 mg, 0.25 mmol) in dry DMF (3 mL) was added dropwise at 0 °C, and it was stirred at room temperature for 8 h. The reaction mixture was poured into ice water leading to the precipitation of crude products. **HBT-Ph-BnB** as a white solid (93.0 mg, 68% yield) was obtained via purification

https://doi.org/10.1021/acs.analchem.3c05718
Anal. Chem. 2024, 96, 3600−3608

by using silica gel column chromatography (petroleum ether/dichloromethane as eluents, v/v = 2:1).

^{1}H NMR (600 MHz, $CDCl_3$, ppm): δ = 8.74 (s, 1H), 8.14 (d, J = 8.0 Hz, 1H), 7.90 (d, J = 7.7 Hz, 1H), 7.74 (s, 7H), 7.45−7.35 (m, 5H), 7.40 (s, 3H), 7.12 (d, J = 7.1 Hz, 2H), 4.63 (s, 2H), 1.36 (s, 12H). ^{13}C NMR (150 MHz, $CDCl_3$, ppm): δ = 163.2, 153.9, 152.5, 140.0, 139.4, 138.1, 137.9, 136.5, 134.8, 132.3, 129.6, 129.0, 128.7, 128.2, 128.0, 127.7, 127.6, 127.3, 126.2, 125.1, 123.2, 121.6, 84.0, 75.7, 25.0. HR-MS (ESI, m/z): calcd for $C_{38}H_{34}BNO_3S$ $[M + H]^+$: 596.2431, found: 596.2402.

Synthesis of Probe HBT-Fl-BnB. To a 100 mL Schlenk flask with a magnetic stirrer, 2-(benzo[d]thiazol-2-yl)-4,6-diiodophenol (239 mg, 0.5 mmol), 9,9-dihexylfluorene-2-boronic acid (567 mg, 1.5 mmol), potassium carbonate (547 mg, 4 mmol) and 1,1′-bis(diphenylphosphino)ferrocene-palladium(II)-dichloride dichloromethane complex (30 mg, 0.037 mmol) were added under N_2, followed by the addition of toluene/H_2O mixture (2 mL/1 mL). The reaction mixture was bubbled with N_2 for 10 min and was heated to reflux at 120 °C for 17 h. After being cooled to room temperature, water and petroleum ether were added, and the organic layer was separated. It was filtered by passing through a pad of Celite and washed with additional petroleum ether. The filtrate was evaporated under reduced pressure and was further purified by using silica gel column chromatography (petroleum/dichloromethane as eluents, v/v = 10:1), affording desired **HBT-Fl** as a white solid (269 mg, 60%).

^{1}H NMR (600 MHz, $CDCl_3$, ppm): δ = 13.1 (s, 1H), 8.01−8.00 (d, J = 8.0 Hz, 1H), 7.98−7.97 (d, J = 2.1 Hz, 1H), 7.96−7.95 (d, J = 7.8 Hz,1H), 7.84−7.80 (m, 3H), 7.77−7.73 (m, 4H), 7.66−7.65 (dd, J = 1.6 Hz, 1.6 Hz, 1H), 7.61 (d, J = 1.2 Hz, 1H), 7.55−7.52 (m, 1H), 7.46−7.44 (m, 1H), 7.39−7.31 (m, 6H), 2.08−1.98 (m, 8H), 1.16−1.08 (m, 24H), 0.80−0.70 (m, 20H).

To a Schlenk tube containing **HBT-Fl** (446 mg, 0.5 mmol) in dry DMF (15 mL) was added NaH (60% in mineral oil, 22 mg, 0.55 mmol) in portions at 0 °C, and the mixture was stirred for 0.5 h. Then, a solution of 4-bromomethylphenylboronic acid pinacol ester (163 mg, 0.55 mmol) in dry DMF (3 mL) was added dropwise at 0 °C, and it was stirred at room temperature for 8 h. The reaction mixture was poured into ice water leading to the precipitation of crude products. **HBT-Fl-BnB** as a white solid (120.0 mg, 82% yield) was obtained via purification by using silica gel column chromatography (petroleum ether/dichloromethane as eluents, v/v = 10:1).

^{1}H NMR (600 MHz, $CDCl_3$, ppm): δ = 8.74 (d, J = 8.0 Hz, 1H), 8.15−8.14 (d, J = 2.1 Hz, 1H), 7.90−7.88 (d, J = 7.8 Hz, 1H), 7.82−7.79 (m, 3H), 7.82−7.70 (m, 6H), 7.66−7.65 (d, J = 1.6 Hz, 2H), 7.53−7.50 (m, 1H), 7.40−7.32 (m, 7H), 7.15−7.14 (d, J = 7.8 Hz, 2H), 4.71 (s, 2H), 2.06−1.99 (m, 8H), 1.32 (s, 12H), 1.16−1.08 (m, 24H), 0.80−0.70 (m, 20H). ^{13}C NMR (150 MHz, $CDCl_3$, ppm): δ = 162.8, 162.9, 161.8, 150.8, 150.6, 150.3, 140.2, 140.0, 138.7, 139.1, 136.5, 136.2, 135.7, 134.0, 131.2, 127.7, 127.4, 126.7, 126.5, 126.1, 125.5, 124.3, 123.0, 122.2, 120.8, 119.2, 119.1, 83.0, 74.5, 54.6, 39.7, 39.6, 30.8, 30.8, 23.0, 24.1, 23.1, 21.8, 13.3. HR-MS (ESI, m/z): calcd for $C_{76}H_{90}BNO_3S$ $[M + H]^+$: 1108.6813, found: 1108.6815.

Biological Application. *Cell Safety Experiment.* In the cytotoxicity experiment, well-formed Raw264.7 cells were first transferred into a 96-well plate (6000 cells/well) and cultured for 24 h to allow cells to adhere completely. Subsequently, Raw264.7 cells were continued with different concentrations of **HBT-Fl-BnB** solution (0, 5, 10, 15, 20, 30, and 50 μM) in the cell culture incubator. After incubation for 24 h, 100 μL of CCK-8 solution (10 μL) to each well was added, and the cells were incubated for another 4 h. The OD value at a wavelength of 450 nm was measured using a BIOTEK ELX80 enzyme-linked immunosorbent assay instrument.

Confocal Microscopy Imaging of Cells. Dual channels for the confocal microscope were used to image the cells treated with **HBT-Fl-BnB**: the first channel (430ch) λ_{em}= 415−515 nm and the second channel (583ch) λ_{ex} = 405 nm and λ_{em} = 550−650 nm.

Exogenous anti-interference experiments of the probe in cells: Raw264.7 cells were stimulated with 10 μM different ROS (H_2O_2, HOCl, NO, $O_2^{\cdot-}$, and $ONOO^-$) or PBS for 30 min, incubated with 10 μM **HBT-Fl-BnB** for 10 min, and imaged under a confocal microscope.

Sensitivity experiments of **HBT-Fl-BnB** in cells: Raw264.7 cells were stimulated with different concentrations of SIN-1 (0, 10, 20, 30, 40, and 50 μM) for 60 min, incubated with **HBT-Fl-BnB** (10 μM) for 10 min, and imaged under a confocal microscope.

Endogenous anti-interference experiments of **HBT-Fl-BnB** in cells: Raw264.7 cells were stimulated with different stimuli for 4 h, incubated with **HBT-Fl-BnB** (10 μM) for 10 min, and imaged under a confocal microscope.

Different stimuli: PBS for 4 h; LPS (1 μg/mL) for 4 h; IFN-γ (50 ng/mL) for 4 h; PMA (10 nmol/L) for 4 h; LPS (1 μg/mL) + IFN-γ (50 ng/mL) for 4 h; LPS (1 μg/mL) + IFN-γ (50 ng/mL) were incubated for 4 h, then induced with PMA (10 nmol/L) for 0.5 h; NO synthase inhibitor AG (1 mmol/L), LPS (1 μg/mL) and IFN-γ (50 ng/mL) for 4 h, and then PMA (10 nmol/L) for 0.5 h.

Fabrication and Imaging of Animal Disease Models. Dual channels for small animal in vivo imaging systems were used to image the mouse treated with **HBT-Fl-BnB**: the first channel (430ch) λ_{em}= 415−515 nm and the second channel (583ch) λ_{ex} = 405 nm and λ_{em} = 550−650 nm.

Eight-week-old female C57BL/6 mice were selected, and at different time points (0, 6, 12, 24, 36, 72 h) after intraperitoneal injection of inactivated *Escherichia coli* (2×10^7 CFU) or the same amount of PBS, **HBT-Fl-BnB** (50 μM, 200 μL) was injected through the tail vein at 30 min before imaging. Then, these mice were imaged with the small animal in vivo imaging systems PerkinElmer IVIS Lumina XR and the Fluoroscopic Navigator 360I System.

HE Sections Staining. Fresh animal tissues were cleaned in normal saline, embedded in an OTC immediately, and sliced in a cryostat with a thickness of 10 μm. First, the sections were fixed in fixative for 1 min and then washed twice with water. They were stained with hematoxylin for 15 min and then washed twice with water. These sections were differentiated with 1% hydrochloric acid ethanol for 5 s, washed with water for 10 min, and stained with eosin for 2 min. Finally, they were dehydrated to be transparent and were examined under an optical microscope after sealing.

RESULTS AND DISCUSSION

Design and Synthesis of Probe HBT-Fl-BnB. To achieve a ratiometric fluorescent probe, our strategy includes the following considerations: (1) Suitable polycyclic aromatic hydrocarbon (PAH) connected to the HBT core at the *ortho* and *para* positions (relative to the OH), which would not only

https://doi.org/10.1021/acs.analchem.3c05718
Anal. Chem. 2024, 96, 3600−3608

alter the π-delocalized ESIPT into the zwitterionic one but also provide an extended π-conjugated system being coupled with ICT from electron-rich PAH to electron-poor benzothiazole; (2) a highly reactive center for $ONOO^-$; and (3) the control of zwitterionic ESIPT by a protecting group. Therefore, the new rationally designed probe, termed as **HBT-Fl-BnB**, consisted of HBT, two FL substituents at the *ortho* and *para* positions of OH, and 4-bromomethylphenylboronic acid pinacol ester (Br-BnB) masking the zwitterionic ESIPT and monitoring the $ONOO^-$ (Scheme 1a).[40]

The synthetic route of **HBT-Fl-BnB** was outlined in Scheme 1b. The Pd-catalyzed cross-coupling of fluorenyl boronic acid with HBT-diiodides **1** efficiently formed **HBT-Fl** in 60% yield. Then, it further reacted with 4-bromomethylphenylboronic acid pinacol ester, affording the desired **HBT-Fl-BnB** in 82% yield. Additionally, to evaluate the effect of different aromaticities (such as Fl, Ph, and H moieties) on the redshift of emission, **HBT-BnB** and **HBT-Ph-BnB** were also synthesized. All synthetic details and characterizations are described in the Experimental Section.

Spectroscopic Properties. We first studied the UV−vis and fluorescence behaviors of **HBT-R-BnB** and **HBT-R** under simulated physiological conditions (10 μM, PBS buffer with 5% THF, and 0.2% Tween 80 at pH = 7.4). As shown in Figure S1, **HBT-Fl-BnB** exhibited a λ_{max} of absorption at 315 nm, while two absorption bands at 315 and 376 nm were found for **HBT-Fl**. Upon excitation, **HBT-Fl-BnB** exhibited a strong fluorescence peak centered at 396 nm (Figure 1a). In

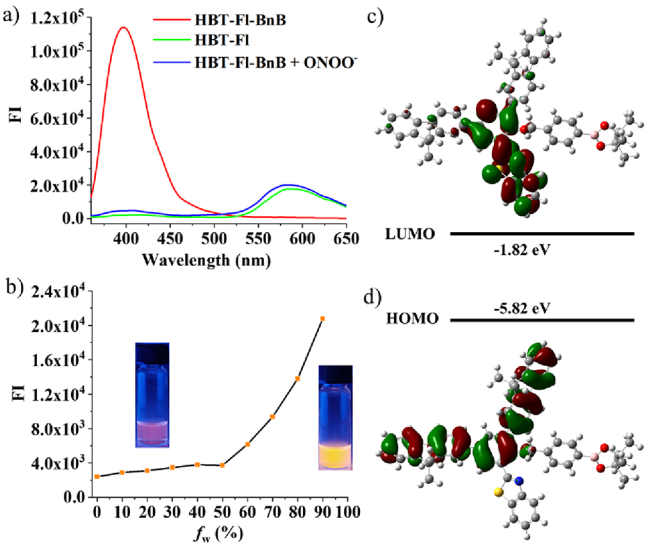

Figure 1. (a) Fluorescence spectra of **HBT-Fl-BnB**, **HBT-Fl**, and **HBT-Fl-BnB** with excess $ONOO^-$ (10 μM, and 10 mM PBS buffer with 5% THF, 0.2% Tween, pH = 7.4, λ_{ex} = 340 nm) and (b) plot of fluorescent intensity of **HBT-Fl** (10 μM) at 584 nm vs water fractions (%, f_w) in the PBS buffer-THF mixture, λ_{ex} = 360 nm. (c, d) DFT calculations of the molecular frontier orbitals and energy levels of the Me derivative of **HBT-Fl-BnB**.

comparison, **HBT-Fl** emitted only a broad peak at about 584 nm involving a zwitterionic ESIPT mechanism according to the previous report.[37] Besides, it also exhibited a solvent polarity-dependent aggregation-induced emission, which was recorded in the PBS buffer-THF mixture by varying the proportions of water (Figures 1b and S2). Fluorescent spectra of **HBT-BnB** and **HBT-Ph-BnB** (Figure S3) clearly indicated that the introduction of **Fl** units did enable a redshift of emission with higher intensity, and a similar redshift effect was also observed for **HBT**, **HBT-Ph**, and **HBT-Fl** (Figure S4). We preliminarily investigated this effect by density functional theory (DFT) calculations at the B3LYP/6-311+G(2d,p) level of theory in vacuo (Figure 1c).[41] The LUMO of **HBT-Fl-BnB** is located at the two Fl units and the phenyl ring at the 2-position of HBT with the energy level of −1.82 eV, and its HOMO mainly occupies the HBT core with the energy level at −5.82 eV. The separation of the frontier molecular orbitals supported an efficient ICT process between the two Fl units and HBT moiety in comparison with that of **HBT-Ph-BnB** (Figure S10), contributing to the strong emission.[42]

Initially, we examined the photostability and chemostability of **HBT-Fl-BnB**. It alone was stable under visible light irradiation and from pH = 4 to 10, suggesting good photo- and chemostabilities (Figures S5 and S6). Upon addition of excess $ONOO^-$, the fluorescence intensity of the peak at 396 nm remarkably decreased, and a new peak at 583 nm appeared (Figure 1a), reaching a relatively steady level within 2 min (Figure S7). The capability of **HBT-Fl-BnB** to quantitatively detect $ONOO^-$ was assessed by using a fluorescent titration method. When varying the concentration of $ONOO^-$ from 0 to 100 μM (0 to 10 equiv to the probe), the gradual decrease of fluorescence at 396 nm and the steady increase of fluorescence at 583 nm were observed (Figure 2a). It enabled

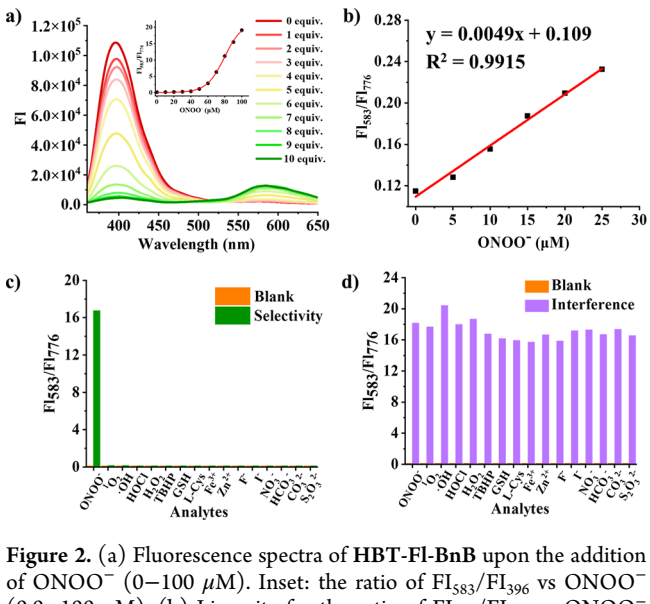

Figure 2. (a) Fluorescence spectra of **HBT-Fl-BnB** upon the addition of $ONOO^-$ (0−100 μM). Inset: the ratio of FI_{583}/FI_{396} vs $ONOO^-$ (0.0−100 μM). (b) Linearity for the ratio of FI_{583}/FI_{396} vs $ONOO^-$ concentrations (0.0−25 μM). Fluorescent intensity ratio (FI_{583}/FI_{396}) of **HBT-Fl-BnB** upon (c) adding $ONOO^-$ or other interfering analytes and (d) adding $ONOO^-$ in the presence of competitive analytes. Test conditions: 10 μM **HBT-Fl-BnB**, 10 mM PBS buffer with 5% THF, 0.2% Tween, pH = 7.4, and λ_{ex} = 340 nm. Other interfering analytes: $ONOO^-$, $^1O_2$, ·OH, HOCl, H_2O_2, NO, TBHP, GSH, L-Cys, Sec, Cys-SSH, Fe^{3+}, Zn^{2+}, F^-, I^-, SO_4^{2-}, NO_2^-, HCO_3^-, CO_3^{2-}, and $S_2O_3^{2-}$.

the ratiometric detection of $ONOO^-$ by measuring the fluorescent intensity ratio of FI_{583}/FI_{396}. As shown in Figure 2b, the ratio of FI_{583}/FI_{396} vs $ONOO^-$ concentration showed an excellent linear relationship from 0 to 25 μM. The linear equation was concluded as $y = 0.0005x + 0.0123$ (R^2 = 0.9949), and the limit of detection (LOD) was 2.1 μM based

https://doi.org/10.1021/acs.analchem.3c05718
Anal. Chem. 2024, 96, 3600−3608

Scheme 2. Proposed Reaction Mechanism of HBT-Fl-BnB toward Detecting ONOO⁻

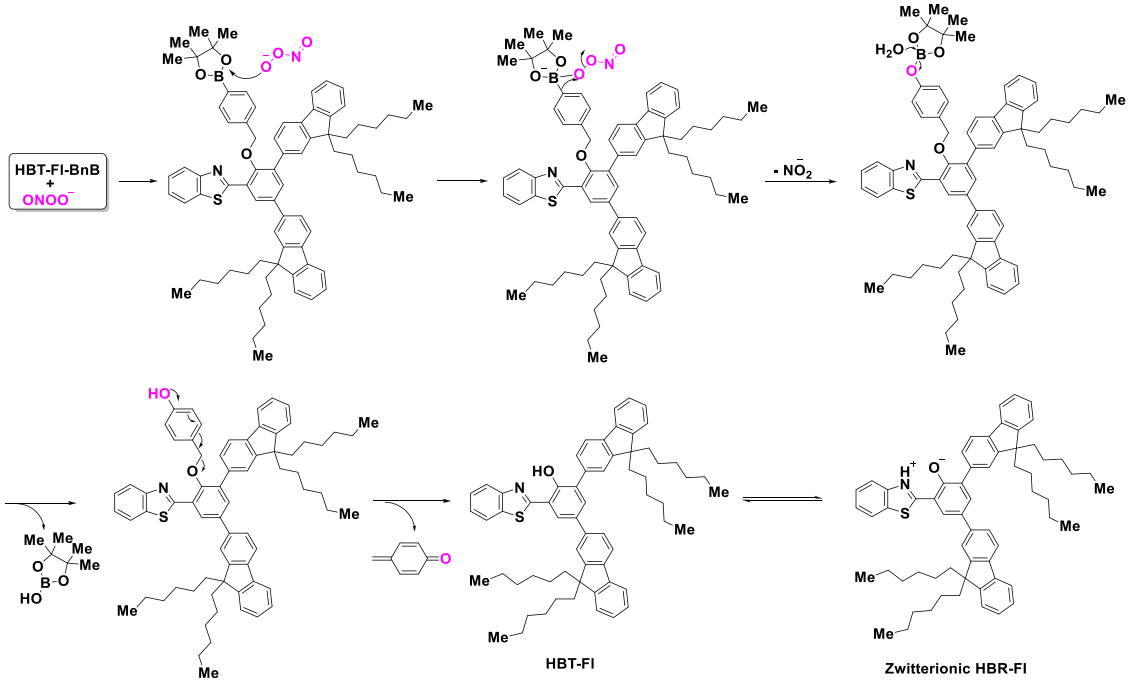

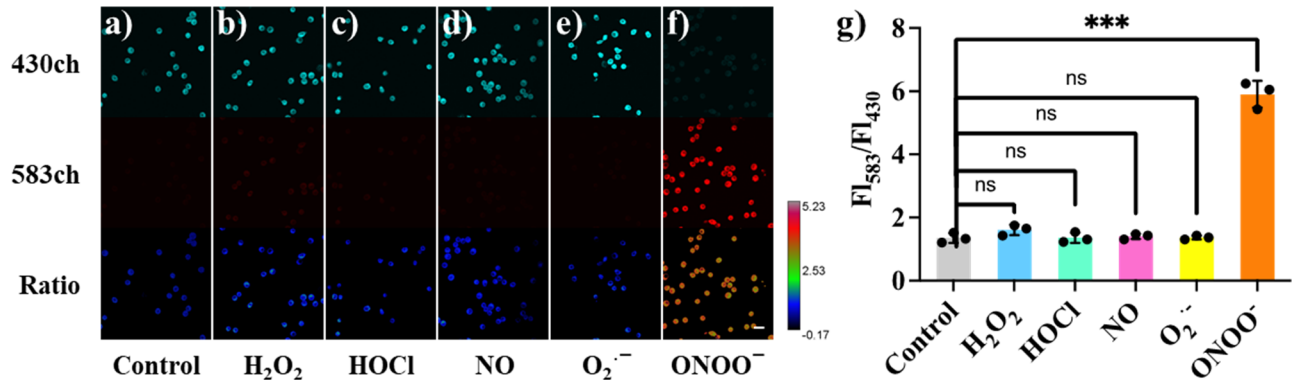

Figure 3. Confocal fluorescence imaging of Raw264.7 cells. (a) Control group: cells were incubated only with **HBT-Fl-BnB**. Cells were stimulated with exogenous ROS/RNS: (b) H_2O_2; (c) HOCl; (d) NO; (e) $O_2^{\cdot-}$; (f) $ONOO^-$ (10 μM in PBS buffer) and then with **HBT-Fl-BnB**. 430ch: λ_{em} = 415−515 nm; 583ch: λ_{em} = 550−650 nm. Ratio images generated from 583ch/430ch. λ_{ex} = 405 nm, scale bar: 20 μm. (g) Normalized average fluorescence intensity of Fl_{583}/Fl_{430}. *** $P < 0.001$. The experiments were repeated three times, and the data are shown as mean (±S.D.).

on LOD = $3\sigma/k$ (σ is the standard deviation of the fluorescent spectrometer, and k is the slope of the correction curve).

Optical Responses of HBT-Fl-BnB toward ONOO⁻. The specificity of **HBT-Fl-BnB** toward $ONOO^-$ was further evaluated in comparison with various potential interfering species including ROS, thiol compounds, and anions (such as $^1O_2$, ·OH, HOCl, H_2O_2, NO, *tert*-butyl hydroperoxide (TBHP), glutathione (GSH), L-cysteine (L-Cys), selenocysteine (Sec), Cys-SSH, Fe^{3+}, Zn^{2+}, F^-, I^-, SO_4^{2-}, NO_2^-, HCO_3^-, CO_3^{2-}, and $S_2O_3^{2-}$, 300 μM). As depicted in Figures 2c and S8, only the addition of $ONOO^-$ led to an enhancement of the ratio of FI_{583}/FI_{396}, whereas other analytes almost resulted in negligible fluctuations. Even when samples of **HBT-Fl-BnB** contained ROS and these interfering analytes at the same time, the specific recognition of $ONOO^-$ was not affected at all (Figures 2d and S9). Additionally, it showed that this ratio of FI_{583}/FI_{396} gradually increased along with the pH varying from 4 to 10 (Figure S6), suggesting an effective sensing of $ONOO^-$ in the cytoplasm (pH ∼ 7.4) and mitochondria (pH ∼ 8.0). In one word, these results indicate that **HBT-Fl-BnB** can serve as an alternative ratiometrically fluorescent probe for the sensitive and selective detection of intracellular $ONOO^-$.

Mechanism Study. To confirm the sensing mechanism of **HBT-Fl-BnB** toward $ONOO^-$, the isolation of possible product obtained from the reaction of **HBT-Fl-BnB** (20 mg) with excess $ONOO^-$ was carried out and further characterized by using the ^1H NMR study. As shown in Figure S11, the proton peak assigned to the methylene group in the BnB moiety at 4.71 ppm disappeared, and a new broad sign proton peak at 13.10 ppm emerged. It was found that this spectrum was the same as that of **HBT-Fl**, proving it as the final product. According to previous literature,[40,43] a proposed reaction mechanism of **HBT-Fl-BnB** involving the cleavage of BnB unit in the presence of $ONOO^-$ is presented in Scheme 2.

Biological Application. *Fluorescent Imaging of Exogenous ONOO⁻ in Raw264.7 Cells.* Before imaging, the cytotoxicity of **HBT-Fl-BnB** against Raw264.7 cells was

https://doi.org/10.1021/acs.analchem.3c05718
Anal. Chem. 2024, 96, 3600−3608

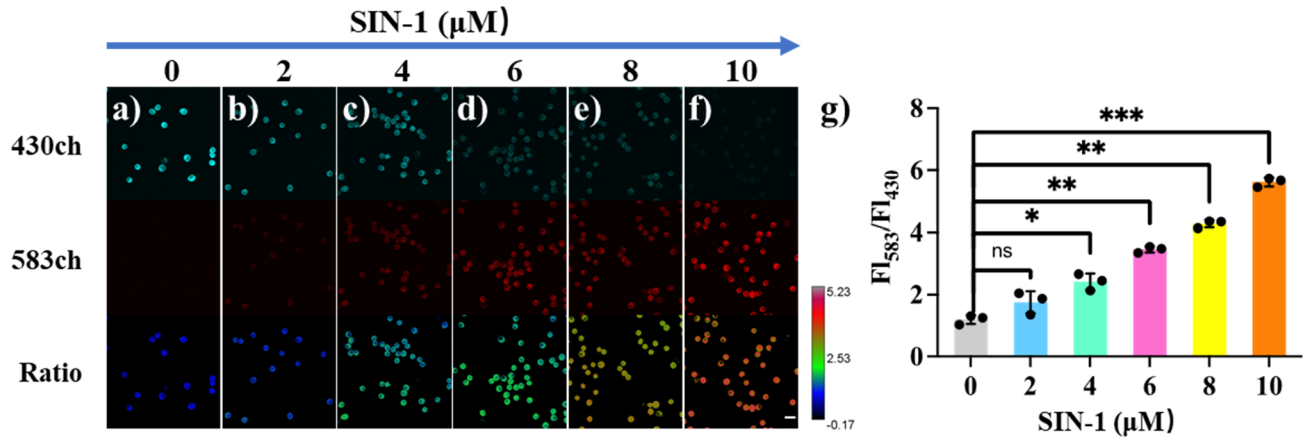

Figure 4. Confocal fluorescence imaging of Raw264.7 cells. Cells were stimulated with different concentrations of $ONOO^-$: (a) 0, (b) 2, (c) 4, (d) 6, (e) 8, and (f) 10 μM and then with **HBT-Fl-BnB**. 430ch: λ_{em} = 415−515 nm; 583ch: λ_{em} = 550−650 nm. Ratio images generated from 583ch/430ch. λ_{ex} = 405 nm, scale bar: 20 μm. (g) Normalized average fluorescence intensity of Fl_{583}/Fl_{430}. * $P < 0.05$, ** $P < 0.01$ *** $P < 0.001$. The experiments were repeated three times, and the data are shown as mean (±S.D.).

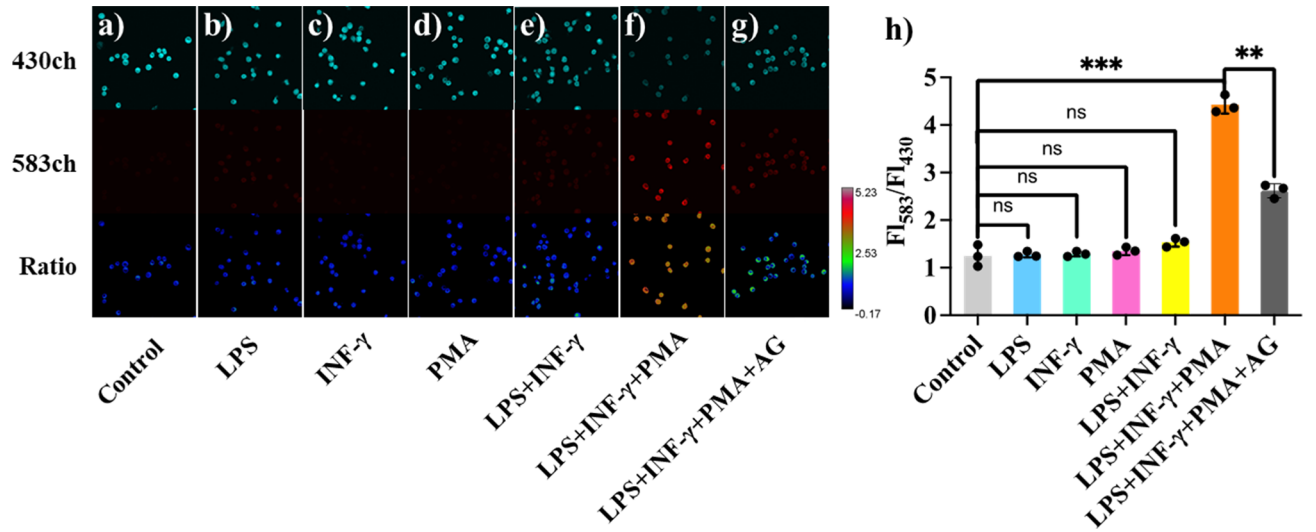

Figure 5. Confocal fluorescence imaging of Raw264.7 cells. (a) Control group: cells were only incubated with **HBT-Fl-BnB**. Cells were stimulated with different stimuli: (b) LPS (1 μg/mL); (c) IFN-γ (50 ng/mL); (d) PMA (10 nmol/L); (e) LPS (1 μg/mL) + IFN-γ (50 ng/mL); (f) LPS (1 μg/mL) + IFN-γ (50 ng/mL) and then with PMA (10 nmol/L); (g) AG (1 mmol/L) + LPS (1 μg/mL) + IFN-γ (50 ng/mL), then with PMA (10 nmol/L), and then further incubated with **HBT-Fl-BnB**. 430ch: λ_{em}= 415−515 nm; 583ch: λ_{em} = 550−650 nm. Ratio images generated from 583ch/430ch. λ_{ex} = 405 nm, scale bar: 20 μm. (h) Normalized average fluorescence intensity of Fl_{583}/Fl_{430}. ** $P < 0.01$ *** $P < 0.001$. The experiments were repeated three times, and the data are shown as mean (±S.D.).

assessed using the standard 3-(4,5-dimethylthiazol-2-yl)-2,5-diphenyltetrazolium bromide assay. As shown in Figure S12, this probe was found to be nearly nontoxic after being treated with cells for 24 h at a high concentration of 20 μM. A concentration of 10 μM was selected to evaluate its capability for imaging exogenous $ONOO^-$ in living cells via dual fluorescent channels (583ch and 430ch). Given the complex environment inside the living organisms, the anti-interference ability of **HBT-Fl-BnB** for specifically sensing $ONOO^-$ in cells was first explored. Raw264.7 cells were incubated without or with different ROS/RNS including H_2O_2, HClO,[44,45] NO, $O_2^{\cdot-}$, and $ONOO^-$ for 30 min and then treated with **HBT-Fl-BnB** for 10 min. As shown in Figure 3a, the control cells that were only incubated with the probe alone showed a strong cyanine fluorescence in 430ch, indicating a good cell membrane permeability of **HBT-Fl-BnB**. The stimulation with H_2O_2, HClO, NO, and $O_2^{\cdot-}$ almost did not change the fluorescent emission (Figure 3b−e). In sharp contrast, the fluorescence dramatically decreased in 430ch, while it concomitantly appeared in 583ch when the cells were treated with exogenous $ONOO^-$ (Figure 3f). Consequently, it suggested a good anti-interference ability of **HBT-Fl-BnB** toward $ONOO^-$ in cells. As shown in Figure 4, the fluorescent intensity ratio of 583ch and 430ch (FI_{583ch}/FI_{430ch}) steadily increased when the cells were incubated with increasing concentrations of $ONOO^-$ released from 3-morpholino-sydnonimine (0 to 10 μM), indicating the potential ratiometric detection of exogenous $ONOO^-$ in living cells.

Fluorescence Imaging of Endogenous $ONOO^-$ in Raw264.7 Cells. The inflammation and oxidative damage are generally observed in many diseases, which are relevant to abnormal expression levels of $ONOO^-$. Therefore, we selected inflammatory Raw264.7 cells to further evaluate whether the probe could image the endogenous generation of $ONOO^-$

https://doi.org/10.1021/acs.analchem.3c05718
Anal. Chem. 2024, 96, 3600−3608

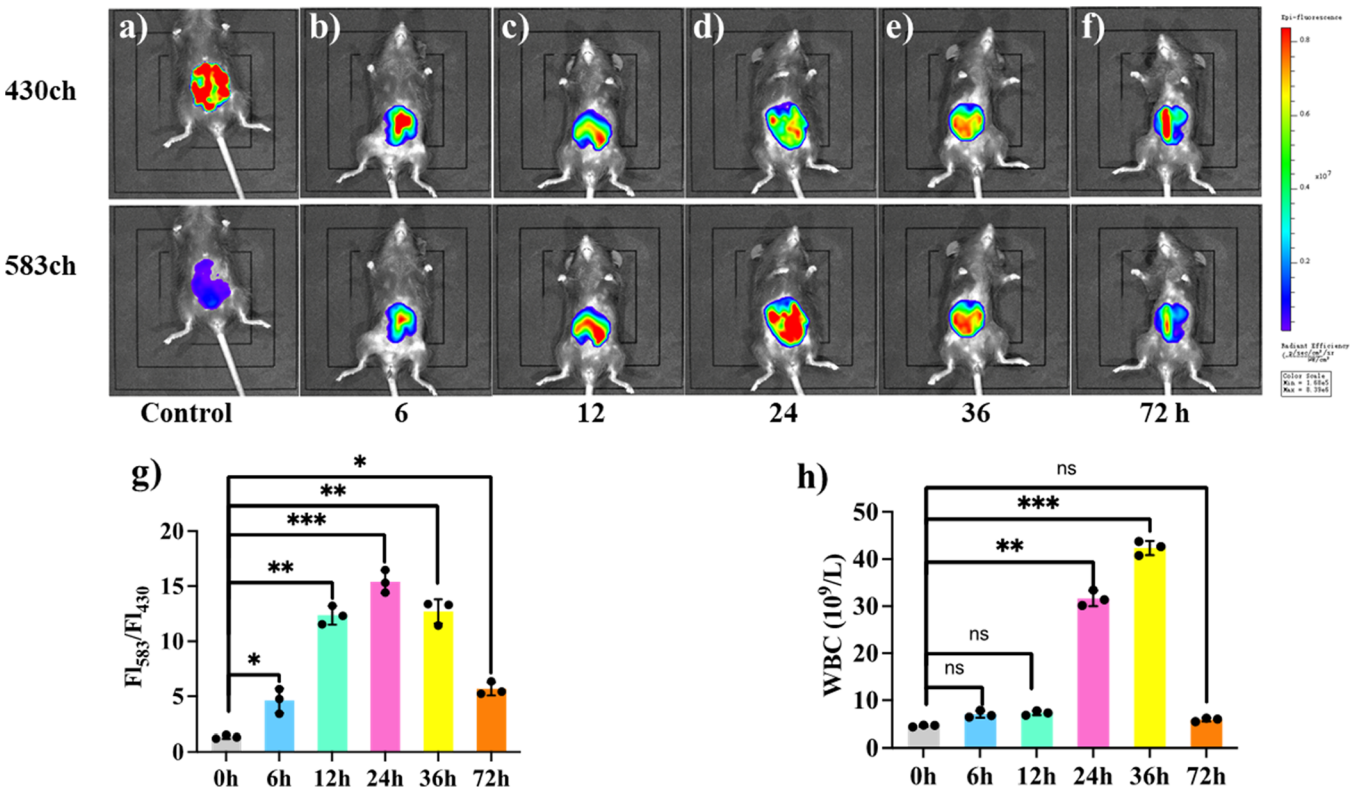

Figure 6. Fluorescence imaging of mice to monitor $ONOO^-$ during *Escherichia coli* caused acute peritonitis. Mice were intraperitoneally injected with inactivated *Escherichia coli* (2×10^7 CFU) and after (a) 0, (b) 6, (c)12, (d) 24, (e) 36, and (f) 72 h, and **HBT-Fl-BnB** (50 μM, 200 μL) was injected through the tail vein. (g) Normalized average fluorescence intensity of Fl_{583}/Fl_{430}. 430ch: λ_{em} = 415−515 nm; 583ch: λ_{em} = 550−650 nm. λ_{ex} = 405 nm. (h) Changes of WBC during acute peritonitis in mice. * $P < 0.05$, ** $P < 0.01$ *** $P < 0.001$. The experiments were repeated three times, and the data are shown as mean (±S.D.).

under various stressors. When the cells were treated by lipopolysaccharide (LPS, mainly stimulating NO synthase, 1 μg/mL), interferon-γ (INF-γ, mainly stimulating NO synthase, 50 ng/mL), and phorbol 12-myristate 13-acetate (PMA, producing superoxide anion, 10 nmol/L) for 4 h followed by incubation with **HBT-Fl-BnB** for 10 min, the fluorescence of 583ch slightly increased, and negligible variations to the emission intensity of 430ch were found in comparison with the control cells (Figure 5b−d vs a). It suggested a very low amount of $ONOO^-$ produced in cells under these endogenous initiators. Note that the combination of LPS/INF-γ/PMA was efficient to upregulate the level of endogenous $ONOO^-$ in cells, and this process was solidly supported by the appearance of strong fluorescence in 583ch accompanied by a significant decrease in 430ch (Figure 5f). When aminoguanidine (AG, the NO synthase inhibitor) was added into the combination of LPS/INF-γ/PMA, the fluorescence ratio of FI_{583ch}/FI_{430ch} obviously reduced (Figure 5g), indicating the down-regulation of endogenous $ONOO^-$ in the presence of AG.

Fluorescence Imaging of Endogenous $ONOO^-$ Expression in Mice. To explore the applicability of **HBT-Fl-BnB** to imaging $ONOO^-$ in vivo, the biosafety of the probe in mice was studied first. It was found that the mice with the tail vein injection of **HBT-Fl-BnB** after 24 h did not show any obvious abnormalities in the blood routine (Figure S16) or hematoxylin-eosin (HE) sections of major organs (Figure S17). Considering the good biosafety, we validated the monitoring of $ONOO^-$ expression in acute peritonitis caused by inactivated *Escherichia coli*.[46] At different time points (0, 6, 12, 24, 36, and 72 h) after intraperitoneal injection of inactivated *Escherichia coli* (2×10^7 CFU) into mice, **HBT-Fl-BnB** (50 μM, 200 μL) was injected through the tail vein. After 30 min, the fluorescence imaging of the mice was performed by the small animal in vivo imaging systems. As shown in Figure 6, it revealed that the expression of $ONOO^-$ during the acute peritonitis increased significantly within 24 h, and then its level gradually decreased. Additionally, the increase in white blood cells (WBCs) in mice was much slower in comparison with that of $ONOO^-$ (Figure 6h), indicating the rapidity and accuracy of **HBT-Fl-BnB** in diagnosing diseases involving $ONOO^-$.

CONCLUSIONS

In summary, a novel ratiometrically fluorescent probe **HBT-Fl-BnB** featuring a zwitterionic ESIPT was first synthesized to detect $ONOO^-$ in vitro and in vivo. An HBT core with two Fl groups at the *ortho* and *para* positions of OH responding to the zwitterionic ESIPT and a boronic acid pinacol ester possessing dual roles of blocking the zwitterionic ESIPT as well as sensing $ONOO^-$ are both presented in **HBT-Fl-BnB**. This designed probe enabled quantitative and ratiometric detection of $ONOO^-$ with high selectivity and sensitivity. Considering the low cytotoxicity and high selectivity of **HBT-Fl-BnB** toward $ONOO^-$, the success in monitoring and imaging of endogenous and exogenous $ONOO^-$ in living cells and mice was obtained. Importantly, the abnormal expression of $ONOO^-$ in vivo induced by inactivated *Escherichia coli* was also confirmed by **HBT-Fl-BnB**, which provided a potential strategy to understand the relevant pathogenic mechanism. We

https://doi.org/10.1021/acs.analchem.3c05718
Anal. Chem. 2024, 96, 3600−3608

envision that this strategy will inspire future probe design with infrared emission.

■ ASSOCIATED CONTENT

Supporting Information

The Supporting Information is available free of charge at https://pubs.acs.org/doi/10.1021/acs.analchem.3c05718.

Materials; instruments; detailed synthetic procedures; ^{1}H NMR, ^{13}C NMR, and HR-MS characterization details; additional photophysical properties; DFT calculations; and cell viability (PDF)

■ AUTHOR INFORMATION

Corresponding Authors

Weiwei Fang − *Jiangsu Co-Innovation Center of Efficient Processing and Utilization of Forest Resources, International Innovation Center for Forest Chemicals and Materials, College of Chemical Engineering, Nanjing Forestry University, Nanjing 210037, China;* orcid.org/0000-0002-2701-5216; Email: wwfang2020@njfu.edu.cn

Fabiao Yu − *Key Laboratory of Hainan Trauma and Disaster Rescue, Key Laboratory of Haikou Trauma, The First Affiliated Hospital of Hainan Medical University and Engineering Research Center for Hainan Bio-Smart Materials and Bio-Medical Devices, Key Laboratory of Emergency and Trauma, Ministry of Education, Key Laboratory of Hainan Functional Materials and Molecular Imaging, College of Emergency and Trauma, Hainan Medical University, Haikou 571199, China;* orcid.org/0000-0003-0073-6299; Email: yufabiao@hainmc.edu.cn

Authors

Zhenkai Wang − *Jiangsu Co-Innovation Center of Efficient Processing and Utilization of Forest Resources, International Innovation Center for Forest Chemicals and Materials, College of Chemical Engineering, Nanjing Forestry University, Nanjing 210037, China; Engineering Research Center for Hainan Bio-Smart Materials and Bio-Medical Devices, Key Laboratory of Emergency and Trauma, Ministry of Education, Key Laboratory of Hainan Functional Materials and Molecular Imaging, College of Emergency and Trauma and Key Laboratory of Hainan Trauma and Disaster Rescue, Key Laboratory of Haikou Trauma, The First Affiliated Hospital of Hainan Medical University, Hainan Medical University, Haikou 571199, China*

Miao Yan − *Jiangsu Co-Innovation Center of Efficient Processing and Utilization of Forest Resources, International Innovation Center for Forest Chemicals and Materials, College of Chemical Engineering, Nanjing Forestry University, Nanjing 210037, China*

Miaomiao Yu − *Jiangsu Co-Innovation Center of Efficient Processing and Utilization of Forest Resources, International Innovation Center for Forest Chemicals and Materials, College of Chemical Engineering, Nanjing Forestry University, Nanjing 210037, China*

Gang Zhang − *Jiangsu Co-Innovation Center of Efficient Processing and Utilization of Forest Resources, International Innovation Center for Forest Chemicals and Materials, College of Chemical Engineering, Nanjing Forestry University, Nanjing 210037, China;* orcid.org/0000-0002-4674-7252

Complete contact information is available at: https://pubs.acs.org/10.1021/acs.analchem.3c05718

Author Contributions

‖Z.W. and M.Y. contributed equally.

Notes

The authors declare no competing financial interest.

■ ACKNOWLEDGMENTS

Financial supports from the National Natural Science Foundation of China (nos. 22101133 and 22264013), the Natural Science Foundation of Jiangsu Province (no. BK20200768), the Natural Science Research Talent Project of Hainan Medical University (grant JBGS202101), the Hainan Province Clinical Medical Center (2021), the Project for Functional Materials and Molecular Imaging Science Innovation Group of Hainan Medical University, and the Nanjing Forestry University are greatly acknowledged.

■ REFERENCES

(1) Pacher, P.; Beckman, J. S.; Liaudet, L. *Physiol. Rev.* **2007**, *87* (1), 315−424.
(2) Szabo, C.; Ischiropoulos, H.; Radi, R. *Nat. Rev. Drug. Discovery* **2007**, *6* (8), 662−680.
(3) Radi, R. J. *Biol. Chem.* **2013**, *288* (37), 26464−26472.
(4) Ischiropoulos, H.; Beckman, J. S. *J. Clin. Invest.* **2003**, *111* (2), 163−169.
(5) Surmeli, N. B.; Litterman, N. K.; Miller, A.-F.; Groves, J. T. *J. Am. Chem. Soc.* **2010**, *132* (48), 17174−17185.
(6) Yu, F.; Li, P.; Wang, B.; Han, K. *J. Am. Chem. Soc.* **2013**, *135* (20), 7674−7680.
(7) Beckman, J. S.; Carson, M.; Smith, C. D.; Koppenol, W. H. *Nature* **1993**, *364* (6438), 584.
(8) Torreilles, F.; Salman-Tabcheh, S. D.; Guérin, M.-C.; Torreilles, J. *Brain. Res. Rev.* **1999**, *30* (2), 153−163.
(9) Sarchielli, P.; Galli, F.; Floridi, A.; Floridi, A.; Gallai, V. *Amino. Acids.* **2003**, *25* (3−4), 427−436.
(10) Peteu, S. F.; Boukherroub, R.; Szunerits, S. *Biosens. Bioelectron.* **2014**, *58*, 359−373.
(11) Zhuang, H.; Li, B.; Zhao, M.; Wei, P.; Yuan, W.; Zhang, M.; Han, X.; Chen, Y.; Yi, T. *Nanoscale.* **2020**, *12* (18), 10216−10225.
(12) Chen, X.; Wang, F.; Hyun, J. Y.; Wei, T.; Qiang, J.; Ren, X.; Shin, I.; Yoon, J. *Chem. Soc. Rev.* **2016**, *45* (10), 2976−3016.
(13) Wang, S.; Chen, L.; Jangili, P.; Sharma, A.; Li, W.; Hou, J.-T.; Qin, C.; Yoon, J.; Kim, J. S. *Coordin. Chem. Rev.* **2018**, *374*, 36−54.
(14) Jiao, X.; Li, Y.; Niu, J.; Xie, X.; Wang, X.; Tang, B. *Anal. Chem.* **2018**, *90* (1), 533−555.
(15) Wu, L.; Sedgwick, A. C.; Sun, X.; Bull, S. D.; He, X.-P.; James, T. D. *Acc. Chem. Res.* **2019**, *52* (9), 2582−2597.
(16) Bezner, B. J.; Ryan, L. S.; Lippert, A. R. *Anal. Chem.* **2020**, *92* (1), 309−326.
(17) Mao, Z.; Xiong, J.; Wang, P.; An, J.; Zhang, F.; Liu, Z.; Kim, J. S. *Coordin. Chem. Rev.* **2022**, *454*, No. 214356.
(18) Ma, Q.; Xu, S.; Zhai, Z.; Wang, K.; Liu, X.; Xiao, H.; Zhuo, S.; Liu, Y. *Chem.—Eur. J.* **2022**, *28* (39), No. e202200828.
(19) Cui, W.-L.; Wang, M.-H.; Yang, Y.-H.; Wang, J.-Y.; Zhu, X.; Zhang, H.; Ji, X. *Coord. Chem. Rev.* **2023**, *474*, No. 214848.
(20) Kwon, J. E.; Park, S. Y. *Adv. Mater.* **2011**, *23* (32), 3615−3642.
(21) Zhao, J.; Ji, S.; Chen, Y.; Guo, H.; Yang, P. *Phys. Chem. Chem. Phys.* **2012**, *14* (25), 8803−8817.
(22) Sedgwick, A. C.; Wu, L.; Han, H. H.; Bull, S. D.; He, X. P.; James, T. D.; Sessler, J. L.; Tang, B. Z.; Tian, H.; Yoon, J. *Chem. Soc. Rev.* **2018**, *47* (23), 8842−8880.
(23) Li, X.; Tao, R.-R.; Hong, L.-J.; Cheng, J.; Jiang, Q.; Lu, Y.-M.; Liao, M.-H.; Ye, W.-F.; Lu, N.-N.; Han, F.; Hu, Y.-Z.; Hu, Y. -H. J. *Am. Chem. Soc.* **2015**, *137* (38), 12296−12303.
(24) Sedgwick, A. C.; Sun, X.; Kim, G.; Yoon, J.; Bull, S. D.; James, T. D. *Chem. Commun.* **2016**, *52* (83), 12350−12352.

(25) Huang, T.; Yan, S.; Yu, Y.; Xue, Y.; Yu, Y.; Han, C. *Anal. Chem.* **2022**, *94* (2), 1415−1424.
(26) Li, Q.; Yang, Z. *Tetrahedron. Lett.* **2018**, *59* (2), 125−129.
(27) Shen, Y.; Zhang, X.; Zhang, Y.; Li, H.; Dai, L.; Peng, X.; Peng, Z.; Xie, Y. *Anal. Chim. Acta* **2018**, *1014*, 71−76.
(28) Wu, L.; Wang, Y.; Weber, M.; Liu, L.; Sedgwick, A. C.; Bull, S. D.; Huang, C.; James, T. D. *Chem. Commun.* **2018**, *54* (71), 9953−9956.
(29) Wu, L.; Han, H. H.; Liu, L.; Gardiner, J. E.; Sedgwick, A. C.; Huang, C.; Bull, S. D.; He, X. P.; James, T. D. *Chem. Commun.* **2018**, *54* (80), 11336−11339.
(30) Guria, U. N.; Gangopadhyay, A.; Ali, S. S.; Maiti, K.; Samanta, S. K.; Manna, S.; Ghosh, A. K.; Uddin, M. R.; Mandal, S.; Mahapatra, A. K. *Anal. Methods-UK.* **2019**, *11* (42), 5447−5454.
(31) Wang, D.; Huyan, Y.; Nan, X.; Li, H.; Sun, S.; Xu, Y. *Chem. Commun.* **2020**, *56* (57), 7925−7928.
(32) Ye, Y.-X.; Chen, X.-Y.; Yu, Y.-W.; Zhang, Q.; Wei, X.-W.; Wang, Z.-C.; Wang, B.-Z.; Jiao, Q.-C.; Zhu, H.-L. *Analys.* **2021**, *146* (21), 6556−6565.
(33) Ding, J.; Yu, L.; Liu, Y.; Yang, Z.; Zhang, Y. *Dyes. Pigments.* **2021**, *191*, No. 109359.
(34) Gu, B.; Wu, C.; Zhang, C.; He, S.; Tang, S.; Li, H.; Shen, Y. *Spectrochim. Acta. A. Mol. Biomol. Spectrosc.* **2021**, *262*, No. 120100.
(35) Sun, Y.; Tang, X.; Li, X.; Kong, X.; Tian, M.; Wang, Y.; Dong, B. *Sens. Actuat. B* **2022**, *353*, No. 131121.
(36) Wang, F. F.; Guo, B. S.; Guo, X. L.; Gu, B.; Shen, Y. M.; Long, J. M. *J. Photoch. Photobio. A* **2022**, *427*, No. 113796.
(37) Shukla, A.; Mai, V. T. N.; Divya, V. V.; Suresh, C. H.; Paul, M.; Karunakaran, V.; McGregor, S. K. M.; Allison, I.; Narayanan Unni, K. N.; Ajayaghosh, A.; Namdas, E. B.; Lo, S. C. *J. Am. Chem. Soc.* **2022**, *144* (30), 13499−13510.
(38) Suzuki, N.; Fukazawa, A.; Nagura, K.; Saito, S.; Kitoh-Nishioka, H.; Yokogawa, D.; Irle, S.; Yamaguchi, S. *Angew. Chem., Int. Ed.* **2014**, *53* (31), 8231−8235.
(39) Wang, C. H.; Liu, Z. Y.; Huang, C. H.; Chen, C. T.; Meng, F. Y.; Liao, Y. C.; Liu, Y. H.; Chang, C. C.; Li, E. Y.; Chou, P. T. *J. Am. Chem. Soc.* **2021**, *143* (32), 12715−12724.
(40) Sikora, A.; Zielonka, J.; Lopez, M.; Joseph, J.; Kalyanaraman, B. *Free. Radic. Biol. Med.* **2009**, *47* (10), 1401−1407.
(41) Frisch, M. J.; Trucks, G. W.; Schlegel, H. B.; Scuseria, G. E.; Robb, M. A.; Cheeseman, J. R.; Scalmani, G.; Barone, V.; Petersson, G. A.; Nakatsuji, H.; Li, X.; Caricato, M.; Marenich, A. V.; Bloino, J.; Janesko, B. G.; Gomperts, R.; Mennucci, B.; Hratchian, H. P.; Ortiz, J. V.; Izmaylov, A. F.; *Gaussian 16, Revision A.03*; Gaussian, Inc.: Wallingford CT, 2016.
(42) Liu, R.; Zhu, G.; Zhang, G. *RSC. Adv.* **2020**, *10* (12), 7092−7098.
(43) Kim, J.; Park, J.; Lee, H.; Choi, Y.; Kim, Y. *Chem. Commun.* **2014**, *50* (66), 9353−9356.
(44) Wang, Z.; Zhang, Y.; Liang, Y.; Li, M.; Meng, Z.; Gong, S.; Yang, Y.; Xu, X.; Wang, S. *Analyst.* **2022**, *147* (10), 2080−2088.
(45) Zhang, Y.; Yang, H.; Li, M.; Gong, S.; Song, J.; Wang, Z.; Wang, S. *Dyes Pigm.* **2022**, *197*, No. 109861, DOI: 10.1016/j.dyepig.2021.109861.
(46) Raby, A. C.; Holst, B.; Le Bouder, E.; Diaz, C.; Ferran, E.; Conraux, L.; Guillemot, J. C.; Coles, B.; Kift-Morgan, A.; Colmont, C. S.; Szakmany, T.; Ferrara, P.; Hall, J. E.; Topley, N.; Labéta, M. O. *Sci. Transl. Med.* **2013**, *5* (185), 185ra164.

https://doi.org/10.1021/acs.analchem.3c05718
Anal. Chem. 2024, 96, 3600−3608